JOURNAL OF AIRCRAFT
Vol. 41, No. 5, September–October 2004

Edge Vortices of a Double-Element Wing in Ground Effect

Xin Zhang* and Jonathan Zerihan†
University of Southampton, Southampton, England SO17 1BJ, United Kingdom

The influence of edge vortices generated by a generic double-element wing on force behaviors are discussed. The wing is equipped with end plates and operates in ground effect. The downforce-vs-height curve is divided into three distinct regions according to ground proximity and flap setting. As the wing is moved from a height in freestream to the ground plane, the downforce first experiences a rapid enhancement (region A). This process is accompanied by the presence of a concentrated vortex off the edge of the side plate and diffuser effect of the wing. At a critical height, the vortex breaks down and its contribution to the downforce is lost. This creates a change in the gradient of the downforce slope. The force enhancement process continues as the height of the wing is reduced (region B); the main diffuser effect is still present. The downforce is lost below a height where the maximum downforce is reached, due to large separation on the wing (region C). The importance of the edge vortices in defining the characteristics of the downforce curve is established.

Nomenclature

b	=	wing span, mm
C_L	=	lift coefficient, $L/q_\infty S$
$C_{P\text{norm}}$	=	normalized spanwise pressure coefficient for lower surface pressures, $c_p \Big/ \int_0^1 c_p \, \mathrm{d}\eta$
c	=	wing chord, mm
c_p	=	pressure coefficient, p/q_∞
h	=	height above ground
L	=	downforce
p	=	pressure
q_∞	=	dynamic head, $\frac{1}{2}\rho_\infty U_\infty^2$
Re	=	Reynolds number, $\rho_\infty U_\infty c/\mu$
S	=	platform area, $b \times c$
U_∞	=	freestream velocity
u, v, w	=	velocity components in x, y, z–axes system
x, y, z	=	Cartesian coordinates; x positive downstream, y positive up, z positive to starboard
η	=	nondimensional span from wing tip, $2z/b$
μ	=	viscosity
ρ_∞	=	freestream density
ω	=	nondimensional planar vorticity $(c/U_\infty)[(\partial v/\partial z) - (\partial w/\partial y)]$
$\omega_{1/4}$	=	nondimensional planar vorticity at flap quarter-chord position
$\omega_{t/e}$	=	nondimensional planar vorticity behind trailing edge

I. Introduction

AERODYNAMICS of a high-lift wing with its suction surface nearest to a moving surface have applications in vehicles using ground effect. The force on the wing points to the ground plane and forms part of the overall aerodynamic grip. Apart from practical concerns, there exist a number of fundamental, challenging issues worthy of serious consideration. These include the transient nature of laminar to turbulent transition position, unsteady wake, suction surface separation, three-dimensional tip flow, and the existence and the role of large edge vortices. The edge vortices are produced off the edge of the side plates that normally accompany a wing in ground operation, between the lowermost edge and the ground plane. The characters of the edge vortex change as the wing is lowered to the ground. They could contribute to the force enhancement process.

In terms of experimental model tests, there are gaps in studies of wings in ground effect, in particular multi-element configurations, which are employed widely. In an earlier study of a double-element wing,[1] the force characteristics and pressures along the center of the wingspan were reported. The force measurements reveal interesting features, such as changes in the gradient of the force-vs-height slope, which have not been adequately addressed. We now attempt to study three-dimensional flow physics, including force enhancement, transition, vortex break down, and so on. Our main focus is on the role of edge vortices in determining the force curve.

II. A Review of Related Work

Past research in wings in ground effect include two-dimensional model tests by Knowles et al.[2] and fixed ground studies by Ranzenbach et al.[3] and Jasinski and Selig.[4] Recently, Zerihan and Zhang performed a series of studies using a single-element wing in ground effect,[5,6] including force, pressure, surface flow, and off-surface measurements using laser doppler anemometry (LDA) and particle image velocimetry (PIV). These single-element wing studies provided a platform for further numerical and multi-element wing studies.

In the past, model tests of multi-element aerofoils in freestream[7–10] have been used as an experimental basis, detailing the flow physics for two-dimensional computational studies. Smith[11] described the five beneficial effects of the gaps between the elements in multi-element flows: slat effect, circulation effect, dumping effect, off-the-surface pressure recovery, and fresh-boundary-layer effect. These generally relate to two-dimensional mechanisms.

The type of multi-element wing examined in the present study typically has a small aspect ratio and is equipped with endplates. Hence three-dimensional features could be important, particularly the vortex system generated off the edge of the endplate. Some relevant studies exist in the area of trailing tip vortex from a wing in freestream, both experimental[12–14] and computational.[15,16] In fact, the vortices observed in the current study are similar in character to the leading-edge vortices studied by Polhamus,[17] using a leading-edge suction analogy, and by Wentz and Kohlman[18] in a model test.

An important feature of the present flow is vortex breakdown. At a high angle of attack, the aerodynamics of vortex breakdown appears in a wide range of documentation for delta wings[19,20] and rectangular wings.[15,20] In addition to breaking down, vortex unsteadiness resulting in vortex wandering is a phenomenon observed

Received 24 March 2003; revision received 27 October 2003; accepted for publication 30 October 2003.

*Professor, Aerospace Engineering, School of Engineering Sciences.
†Research Student, Aerospace Engineering, School of Engineering Sciences.

in some work.[12,13,21] The motion of a trailing vortex near the ground has been investigated by Harvey and Perry[22] via experiments in a moving ground wind tunnel.

No studies have been found commenting on the interaction of a vortex from an upstream element on the downstream element of a wing, an area relevant to the current research. Storms et al.[23] were the first to perform an experimental study into the flowfield about a part-span flap. In essence, the wing, with a half-span Fowler flap, was tested as a two-dimensional aerofoil, that is, with tip losses only from the inboard edge of the flap. Chordwise pressures near the (inboard) tip show a small reduction in pressure, and a more significant increase in suction over the rear portion of the flap, when compared to results far from the tip. However, the suction peak, over the fore portion of the flap, reduces. The effect of the (flap) tip vortex rolling up on the flap tip is to induce a higher velocity region. Sectional lift coefficients show that, overall, there is a loss in lift on the flap as the tip is approached. More recent studies over similar part-span flap configurations[15,24–26] all show the saddle-type pressure distributions near the flap tip, some acknowledging that this is due to the direct influence of the tip vortex.

III. Description of Study

A. Methods and Facility

A generic double-element wing is employed in wind-tunnel model tests (see Fig. 1). The origin of the coordinate system used in the study is located at the leading edge of the wing. A detailed description of the main element coordinates was given by Zerihan and Zhang in Ref. 5 and the flap in Ref. 1. To provide a complete database, a range of measurements were performed, which included on-surface oil flow, force balance, surface pressure taps, and off-surface particle image velocimetry. Details of the tests can be found in Ref. 1.

Tests were performed in the Southampton low-speed 2.1×1.7 m wind tunnel. The tunnel is of a conventional closed-jet, closed-circuit design. At 30 m/s, the freestream turbulence is 0.2%. For correct modeling of the ground plane, the tunnels are equipped with a large, moving belt rig.

B. Model

The main element has a span of 1100 mm and a constant chord of 223.4 mm. The span corresponds to less than 75% of the width of the moving belt to minimize effects at the edge of the belt. The element features a finite trailing edge, corresponding to $0.007c$. The profile is a development of GA(W) profile, type LS(1)-0413 MOD.[5] The flap features a thin profile over the aft portion of the wing. A constant chord of 165.7 mm is employed, the aft of which 35 mm approximately is the thin region, 1 mm thick. Generic endplates were used throughout testing, the geometry of which was chosen to allow the wing to be tested at very low ground heights, of dimensions $400 \times 170 \times 4$ mm. An optimization exercise was performed[1] to set the flap gap and overlap. A total of 202 taps were built into the model, 125 on the main element. The taps are arranged into three groups: one chordwise group located near the semispan, another near the tip, and one spanwise group at the quarter-chord position on both the main element and the flap.

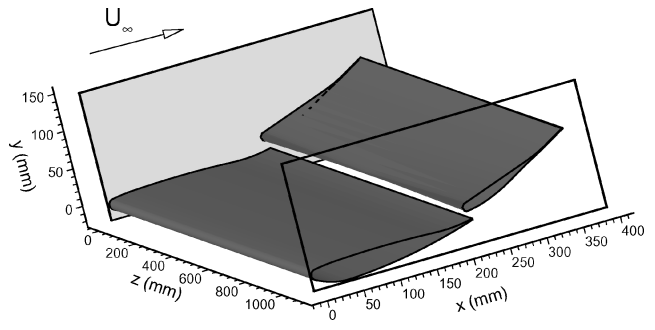

Fig. 1 Schematic of double-element wing in ground effect.

C. Test Conditions

The tests were performed with free transition condition, for a range of heights from $h/c = 1.974$ to less than 0.05 above the ground. The height was defined by the distance from the ground to the lowest point on the wing, with the wing incidence set to 14.1 deg. Two flap settings were used; the datum (or low flap angle) and a flap deflection of +9.5 deg. The point about which the flap was rotated was at a location of $x/c = 0.567$, $y/c = 0.076$, that is, 2 mm downstream from the leading edge of the flap. For the datum deflection, the incidence of the wing is 14.1 deg, with the main element set at an incidence of 1 deg.

All tests were performed at a constant dynamic pressure of 56.25 mm water, corresponding to $U_\infty \approx 30$ m/s the Reynolds numbers are in the range $0.735–0.765 \times 10^6$.

D. Errors and Uncertainties

The incidence of the wing was set to within ± 0.005 deg, and the height above ground was set to within ± 0.2 mm. The tunnel speed was run at a constant dynamic pressure of 56.25 mm water ± 0.05 mm. The uncertainties in C_L were calculated using the addition method and a 95% confidence, the worst case occurring at a height of $0.056c$ and corresponding to a C_L of 1.678 ± 0.009. Uncertainties in the surface-pressure results were calculated for the individual taps using the root-sum-square method; the worst case corresponded to a c_p of ± 0.035. The short-term repeatability was investigated; the highest uncertainties were found to be at the suction peak and the transition bubble, the worst corresponding to a c_p of ± 0.075.

IV. Results

Although both fixed-transition and free-transition cases are investigated in the study, we only report the free-transition cases because they are the most widely used. Of the three distinct regions of the downforce-vs-height curve,[1] we now focus on the changes in the force enhancement region. The loss of downforce is attributed to large separation of the suction surface[1] and will not be the focus of attention in this paper.

A. Surface Streaklines

Surface streaklines were observed at heights of $h/c = 0.395$, 0.263, 0.211, 0.158, and 0.105. Selected results are given in Fig. 2. Only one-half of the span is included. For the low flap angle, transition occurs over most of the span of the main element. Toward the center of the wing, the position of the transition does not vary much. At $h/c = 0.263$, separation bubbles are seen on both the main element and the flap. Measured at one chord length from the tip, the extent of the separation bubble is between 14 and 17% on the main element and 76 and 80% on the flap. The transition bubble extends to the tip but is three-dimensional near the tip. At a greater height of $h/c = 0.395$ (not shown), the numbers are 12–14% on the main element and 74–78% on the flap, within the measurement uncertainties. At a lower height of $h/c = 0.211$, we observe no transition bubble near the tip of the main element. Instead there exists a strong three-dimensional transition region. At one chord length from the tip, transition starts at 11% on the main element and a separation bubble lies between 74 and 78% on the flap. At $h/c = 0.158$, the presence of a transition bubble (closed region of separation) near the center of the wing can still be detected. However, its size and spanwise extent is reduced. On the main element, transition now appears at $x/c = 13\%$. Near the tip, a three-dimensional transition region exists and it occurs much later. On the flap, the transition lies between $x/c = 73$ and 77%. At the lowest height of $h/c = 0.105$, a transition bubble is not observed at one chord length from the tip and transition occurs at $x/c = 22\%$ on the main element. A transition bubble is present on the flap between $x/c = 72$ and 76%.

There is a crossflow presence on the main element, toward the center of the wing. This is attributed to the pressure difference across the endplate, which forces the flow inboard. However, the inboard crossflow is not observed on the flap. Very close to the tip, a crossflow directed outward marks the formation of the main vortex on the main element and the effect of the edge vortex, hence the outward

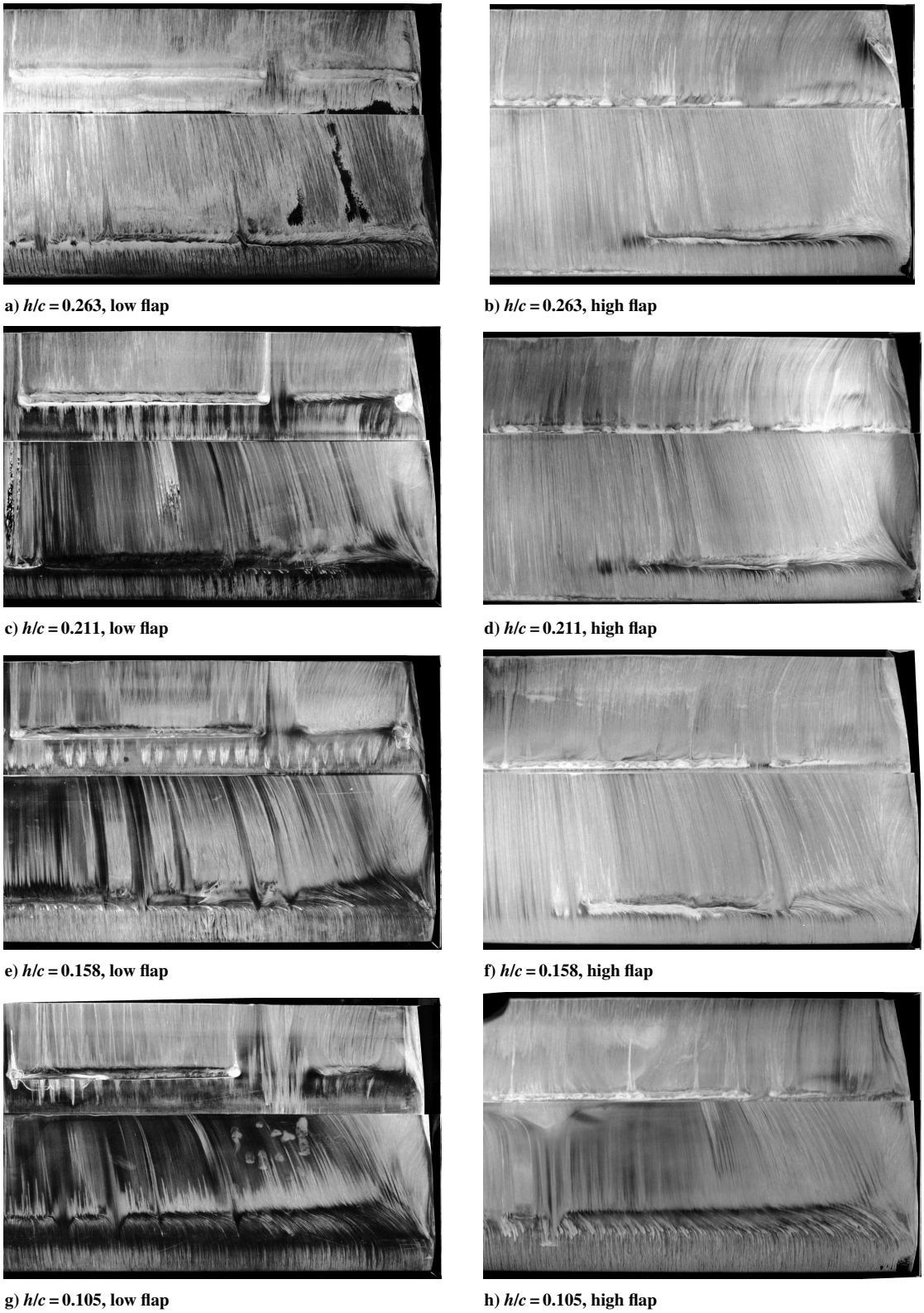

a) $h/c = 0.263$, low flap

b) $h/c = 0.263$, high flap

c) $h/c = 0.211$, low flap

d) $h/c = 0.211$, high flap

e) $h/c = 0.158$, low flap

f) $h/c = 0.158$, high flap

g) $h/c = 0.105$, low flap

h) $h/c = 0.105$, high flap

Fig. 2 Oil flow visualization on suction surface showing leading edge at the bottom of each panel. Flow is from bottom to top. The center of the wing is to the left and the tip to the right.

crossflow on the flap near the tip. At the flap tip, surface streaklines show the presence of a secondary corner vortex, as can be seen in the region between the transition bubble and the endplate. At $h/c = 0.211$, the crossflow on the main element is more extreme, both directed toward the center and in the vortex region. The secondary corner vortex on the flap tip is stronger. The flow lines at the trailing edge of the flap show a greater crossflow as flow is entrained into the main vortex. At $h/c = 0.105$, there is a greater three-dimensionality to the flow on the main element and the crossflow pulling the flow to the center of the wing from outside the vortex is stronger. Near the trailing edge of the flap, the crossflow appears similar or possibly slightly less than that at $h/c = 0.211$. For all the results, the flow patterns on the surface of the flap do not show the direct presence of the main wing edge vortex, only the effect of it.

The generation of an edge vortex is the result of a pressure difference across the endplate and separation of flow on the edge of the

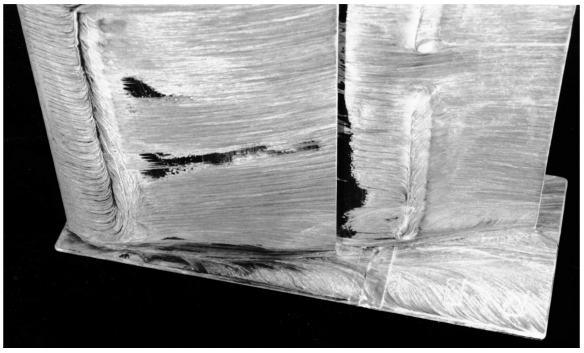

a) $h/c = 0.263$, concentrated edge vortex

b) $h/c = 0.105$, vortex breaking down

Fig. 3 Oil flow visualization on endplate showing leading edge at the left of each panel, low flap angle.

plate. As the vortex evolves downstream in the region of pressure recovery toward the trailing edge of the wing, it faces the likelihood of vortex breaking. As the height is reduced, the pressure recovery demand is much more severe and the vortex breaking would occur earlier. In Fig. 3, the surface streaklines on the endplate suggest that the edge vortex is concentrated at the height of $h/c = 0.263$ (Fig. 3a). However, at $h/c = 0.105$ (Fig. 3b), the sudden divergence of the surface streaklines at around $x/c = 45\%$ indicates the vortex is breaking down. The position of transition near the tip is delayed on the main element. This can be attributed to the low pressure recovery demand near the tip (see later discussion).

In Fig. 2 the high-flap-angle results are also included. On the main element, transition at the leading-edge accounts for a significant portion of the span. In the left portion of the image, the leading-edge bubble can be seen, and on the right, the bubble is farther back, between $x/c = 0.11$ and 0.18 at $h/c = 0.211$. This portion of the wing with leading-edge transition reduces as the ground height is reduced. At $h/c = 0.395$, it is approximately 57% of the span. This reduces to 46% at $h/c = 0.263$, 36% at $h/c = 0.211$, and 20% at $h/c = 0.158$, to virtually zero at $h/c = 0.105$. The transition location for the flap is now very close to the leading edge at $x/c \approx 0.58$. This was found to be the case for all heights tested for the high flap angle.

On the main element, the crossflow directed to the wing center is greater for the lower height case. Again, there is a secondary corner vortex that exists on the flap, very close to the tip. Near the trailing edge of the flap, there is a greater deviation from the streamwise direction for the flow at $h/c = 0.211$, highlighting the effect of the edge vortex that originates from the main element being stronger for this height. As with the low flap angle, the edge vortex begins to break as it evolves downstream, an example of which is given in Fig. 4.

B. Force Behaviors and Surface Pressures

The overall force behaviors were reported by Zhang and Zerihan[1] and will not be repeated here. To aid in the discussion of the edge vortex effect, the force curves are divided into three regions (Fig. 5), which show the height range, together with additional annotations (to be discussed later). In this study we shall concentrate on regions A and B, because they lie in the operation range of height variation.

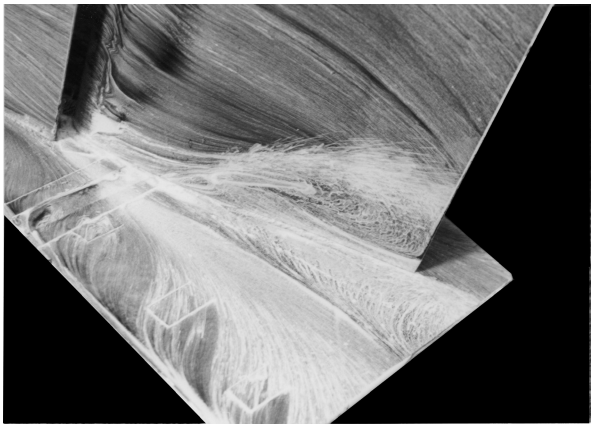

Fig. 4 Vortex breaking at $h/c = 0.263$, high flap angle.

1. *Spanwise Pressures*

The spanwise pressures on the main element indicate that the flow is three-dimensional near the tip (Fig. 6). The suction on the lower surface increases rapidly from the tip as the central portion of the wing is approached. The flow over the upper surface does not change significantly as the height is changed, but the suction surface results vary greatly with the height. This particular feature suggests that the wing in ground flow can be viewed as a diffuser in ground flow. The high flap angle produces a significant increase in lower surface suction and a very small change in upper surface pressures. The distribution of suction does not appear to be as smooth as the results at the low flap angle; at $\eta \approx 0.15$ and 0.75, bumps can be seen, especially at the large heights.

The spanwise pressures on the lower surface of the main element have been normalized by the integral of the pressures with respect to the spanwise position, and the distributions plotted in Fig. 7a, where the normalized pressure coefficient, C_{Pnorm}, would correspond to -1 for the case where the flow is entirely two-dimensional. For the low flap angle, it can be seen that from $\eta \approx 0.73$ a small region of flow that does not feature large spanwise pressure gradients is present at all heights. Outboard of this point, losses in the pressure coefficient are found over the entire region. The flow is three-dimensional over approximately the outer two-thirds. The (normalized) pressure gradients increase over the outer region A as the height is reduced, as the flow would appear to become increasingly three-dimensional. For the high flap angle, Fig. 7b, a broadly similar effect is seen. However, at the smaller heights, the region of flow reduces at the center of the element over which the pressures are approximately constant and appears to have disappeared for the lowest height. Slight irregularities exist, as seen in the spanwise pressure distributions at the high flap angle at $\eta \approx 0.15$ and nearer to the center, at a few heights. It must be noted that the normalized spanwise pressure distributions have been calculated using a single streamwise pressure at the quarter-chord position and are not equivalent to the spanwise variation of loading.

At $h/c = 1.974$, there is some variation in the pressure over the semispan on the lower surface of the low-angle flap (Fig. 8). Near the center, that is, inboard of $\eta = 0.83$, there is a slight reduction in pressure. Near the tip, outboard of $\eta \approx 0.2$, there is a gradual increase in suction, and at the tip there is a finite suction of magnitude slightly higher than the suction over the mid-semispan portion of the flap. The upper surface flow has a relatively constant pressure, with a small dip at $\eta = 0.32$. The dip at this position is caused by the supporting struts attached to the pressure surface. As the height is reduced until $h/c = 0.211$, the suction increases over the central portion from $\eta \approx 0.3$. Over the tip region, the suction also increases. However, for each height, the increment in suction near the flap tip increases compared to the further inboard region. At $h/c = 0.211$, $c_p \approx -1.4$ over the inboard portion of the flap lower surface (i.e., ignoring the very center). The increase near the tip is large, at which $c_p \approx -2.3$. There is a very small reduction in upper surface pressure as the height is reduced. At smaller heights, the trend as the height reduces is different. The suction over the inboard

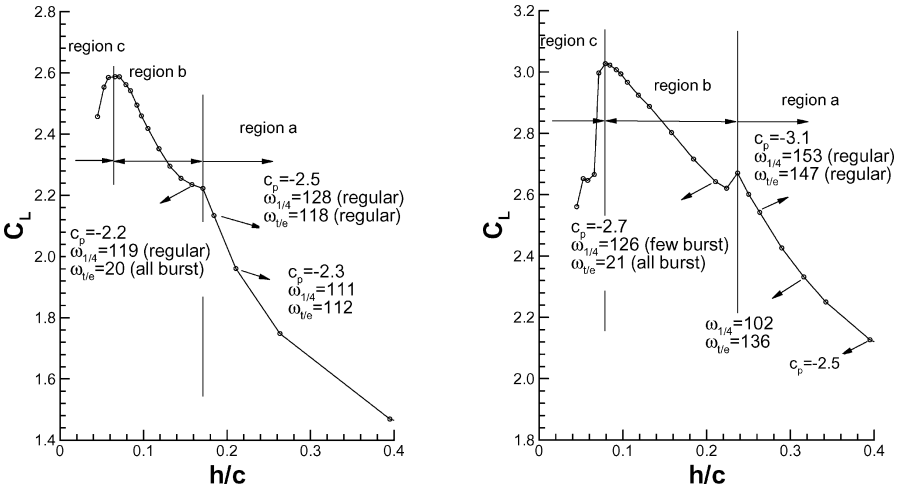

a) Low flap angle **b) High flap angle**

Fig. 5 Downforce curve with ground height, including flow regions and features.

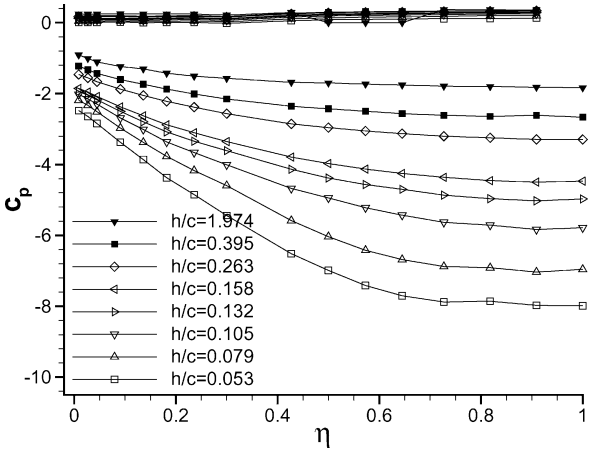

a) Low flap angle

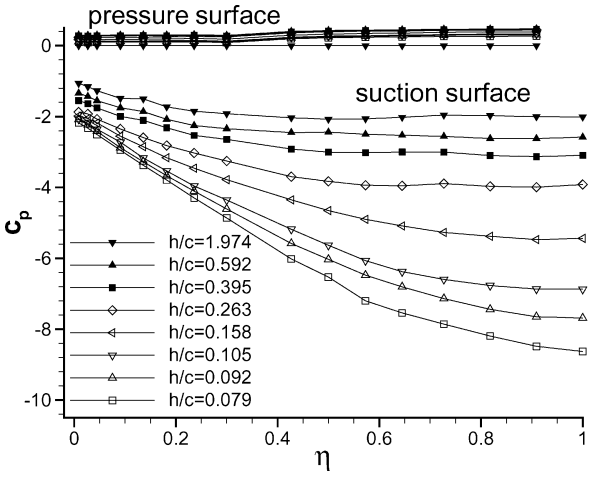

b) High flap angle

Fig. 6 Spanwise surface pressures on main element at quarter-chord position.

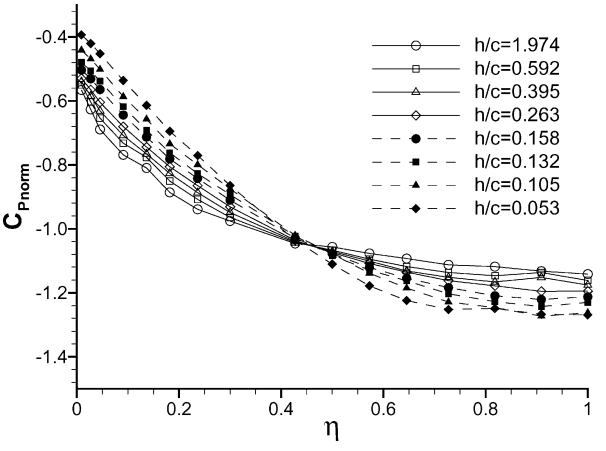

a) Low flap angle

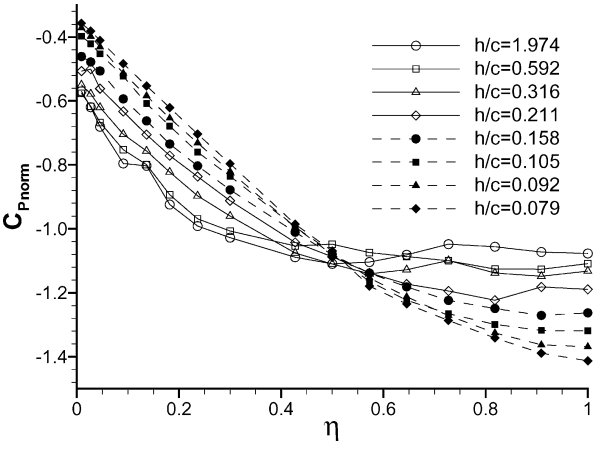

b) High flap angle

Fig. 7 Normalized spanwise suction surface pressures on main element.

portion stays relatively constant, with a slight trend of reducing suction with increasing ground proximity, which is especially visible in the $h/c = 0.053$ case. However, the reduction in height has an adverse effect on the suction increase near the tip. The magnitude of this reduces, and for the $h/c = 0.053$ case this is reduced sufficiently that the suction in this region is less than that found farther inboard. On the upper surface, a slight trend of decreasing pressure with decreasing height can be seen. The values of the maximum suction near the flap tip are indicated in Fig. 5.

For the high flap deflection at $h/c = 1.974$, Fig. 9, the suction over the inboard portion (ignoring the center) of the lower surface is greater than the low flap angle: $c_p \approx -1.2$ compared to $c_p \approx -0.8$ for the low flap angle. The characteristics near the tip are qualitatively similar; however, the magnitude of the increase in suction is bigger for the high flap angle. The suction near the tip corresponds to $c_p \approx -1.7$ compared to $c_p \approx -1.1$ for the low flap angle. The increase in suction from the inboard portion to the tip is therefore greater for the high flap angle. As the height reduces to $h/c = 0.263$, the suction over the inboard portion increases, but not as rapidly as

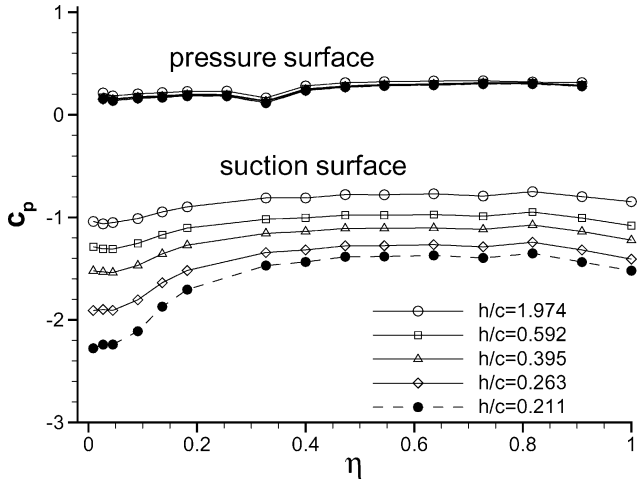

a)

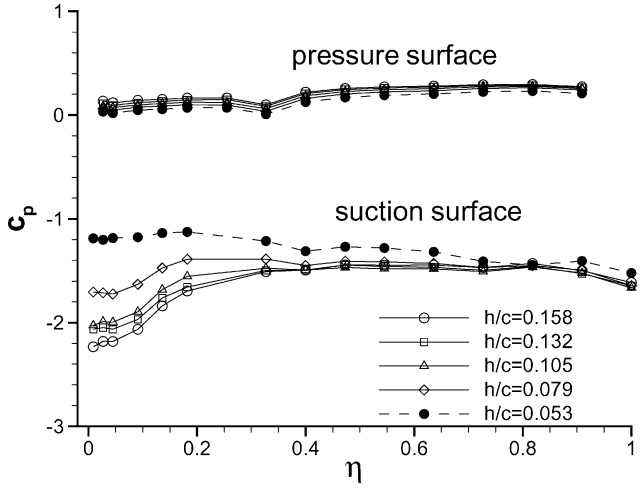

b)

Fig. 8 Spanwise surface pressures on flap at quarter-chord position for low flap deflection: a) concentrated vortex and b) vortex breakdown.

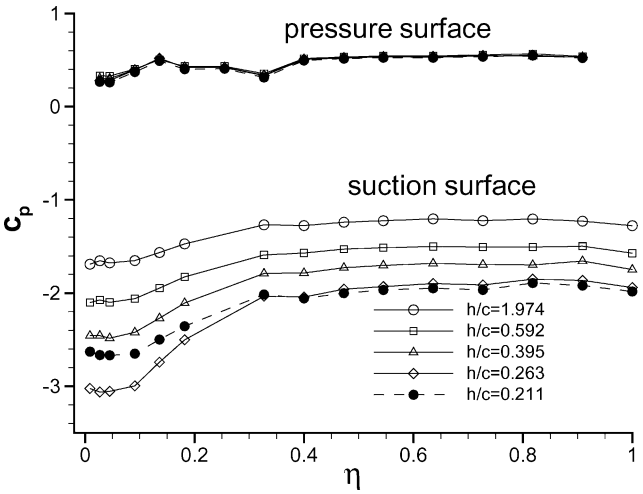

a)

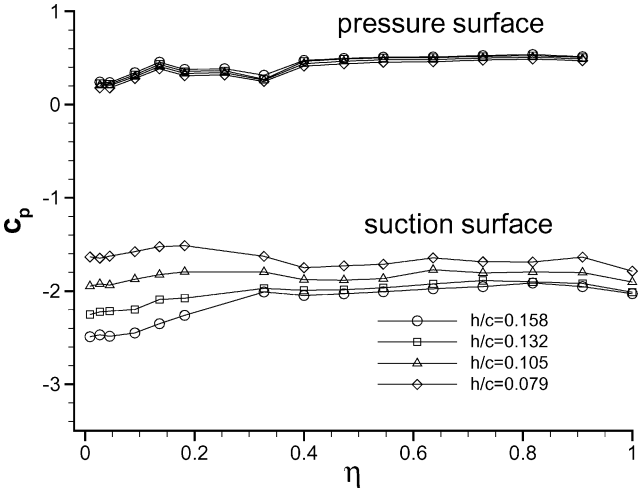

b)

Fig. 9 Spanwise surface pressures on flap at quarter-chord position for high flap deflection: a) concentrated vortex and b) vortex breakdown.

those near the tip. At this height, the suction near the tip is greatest and corresponds to a c_p greater than -3. At smaller heights, the suction over the inboard portion reduces. Moreover, the suction near the tip reduces more significantly such that, at $h/c = 0.079$, the spanwise loading near the tip is less than that over the central portion. Again, the upper surface pressures reduce slightly with reducing height.

2. Chordwise Pressures

At a typical region A height of $h/c = 0.395$, the lower surface suction on the main element is reduced at the tip for the low flap deflection (Fig. 10a). There appears to be very little difference in the suction at the trailing edge of the main element; that is, the boundary layer is dumped at the same velocity. For the center taps, the maximum overall suction on the element is found in the spike very close to the leading edge. Although the spike is still present for the tip taps, it is not as prominent, and the magnitude of the suction is less than at the suction peak at $x/c = 0.08$. On the flap lower surface, the suction is slightly larger near the tip than at the center for the entire mapped chordwise range. On the upper surface, the pressures are reduced by a broadly constant amount over both the main element and the flap. At the high flap angle (Fig. 10b), a loss in suction is again present over the main element lower surface from the center to the tip. On the flap, the suction generated is larger at the tip compared to the center. The magnitude of the increase is greater than that for the low flap angle. The upper surface pressures reduce similarly from the center to the tip.

Figures 10c and 10d show the results at a height of $h/c = 0.105$, a typical height for region B flows. For the low flap angle, the lower surface suction on the main element is again significantly reduced from the center to the tip. The loss in suction from center to tip is greater than the height of $h/c = 0.395$. The maximum suction is at the suction peak at $x/c = 0.10$ for the main element center and the tip. On the flap lower surface, the suction generated at the tip is lower than that at the center, for the region to $x/c \approx 0.65$. Downstream of this, the suction at the tip is a small amount greater than at the center. On the upper surface, the pressure reduces from the center taps to the tip taps. At the high flap angle, results follow the same trend as for the low flap angle.

C. Edge Vortices

The surface flow studies highlighted an area of the flow requiring further studies. The edge vortex was mapped to explain the these results and, in turn, the direct performance of the wing at different heights. Two streamwise locations were examined for each of the flap angles. The first was at the quarter-chord position on the flap (i.e., at a location of $x/c = 0.672$) for exact comparison with the flap spanwise taps. This study was made possible by building a 2-mm vertical slot on the endplate. The second location was at $x/c = 1.092$, that is, behind but close to the endplate. Table 1 lists the maximum mean-flow vorticity in the vortex core.

1. Mean Flow

Figures 11a and 11b show vorticity contours at the two locations for a height of $h/c = 0.211$ in region A for the low flap angle. Some reflections are present, which cause noise in the results (Fig. 11a).

The results at the flap quarter-chord show the vortex core to have a maximum vorticity of $\omega = 111$ (see Table 1 and Fig. 11a). There is a shear layer on the outer edge of the endplate that increases strength to the endplate lower edge; this then rolls up, feeding the vortex. The approximate location of the vortex core is at $z/c = 0.04$, $y/c = -0.04$; it is near the lower edge of the main element and close to the inner edge of the endplate. There is evidence of a secondary shear layer on the inner edge of the endplate, of negative vorticity, at the same height as the core. This is due to the induced velocity from the vortex and the shear on the endplate surface. There is also a region of negative vorticity on the ground, below the vortex, due to the induced crossflow velocity from the vortex and the shear due to the ground. Behind the endplate (Fig. 11b), the vortex is of comparable strength: $\omega = 112$. The shear layer feeding the vortex is well resolved and arises from the lower portion of the outer edge of the endplate. Although the maximum vorticity is similar to that at the quarter-chord, the region of positive vorticity defining the overall vortex size has grown. An effect of this is that the core has moved away from the endplate surface and is now at $z = 0.13$, $y = -0.04$. The induced areas of secondary shear are still present, behind the endplate and on the ground. It was noted that the vortex remains concentrated and its strength increases as the height is reduced.

Table 1 Maximum vorticity in edge vortex[a]

	Low flap deflection		High flap deflection	
h/c	$\omega_{1/4}$	$\omega_{t/e}$	$\omega_{1/4}$	$\omega_{t/e}$
0.395	80	71	——	128
0.316	102	——	102	136
0.263	104	105	153	147
0.211	111	112	126	21
0.184	128	118	——	——
0.158	119	20	53	21
0.105	30	14	30	19
0.053	n/a	n/a	n/a	n/a

[a]$\omega_{1/4}$: flap quarter-chord position; $\omega_{t/e}$: behind trailing edge.

Figures 11c and 11d give the results at a typical height in region B, at $h/c = 0.158$ at the quarter-chord. The vortex shown in Fig. 11c now has a reduced strength from the maximum at $h/c = 0.184$ in region A (Table 1). It also appears a little larger than that shown in Fig. 11a. Again, this vortex has induced velocities, and the inner surface of the endplate and the ground have stronger negative vorticities in these regions. In contrast to the previous trend, the results behind the endplate do not show the presence of a strong vortex core. The vortex is significantly larger than at the greater heights but is at a significantly reduced strength; it appears to have diffused drastically. The maximum measured vorticity corresponds to $\omega = 20$. The rollup of the shear layer from the endplate outer edge is still present. It seems that the region of shear on the endplate inner edge is of a slightly reduced strength than at greater heights. However, the negative vorticity on the ground appears to be stronger than that at the greater heights. At the lower height of $h/c = 0.105$, the results at the quarter-chord also show a weak, diffused vortex (not included).

For the high flap angle, typical results in region A are given in Figs. 12a and 12b. At a height of $h/c = 0.263$, the maximum vorticity

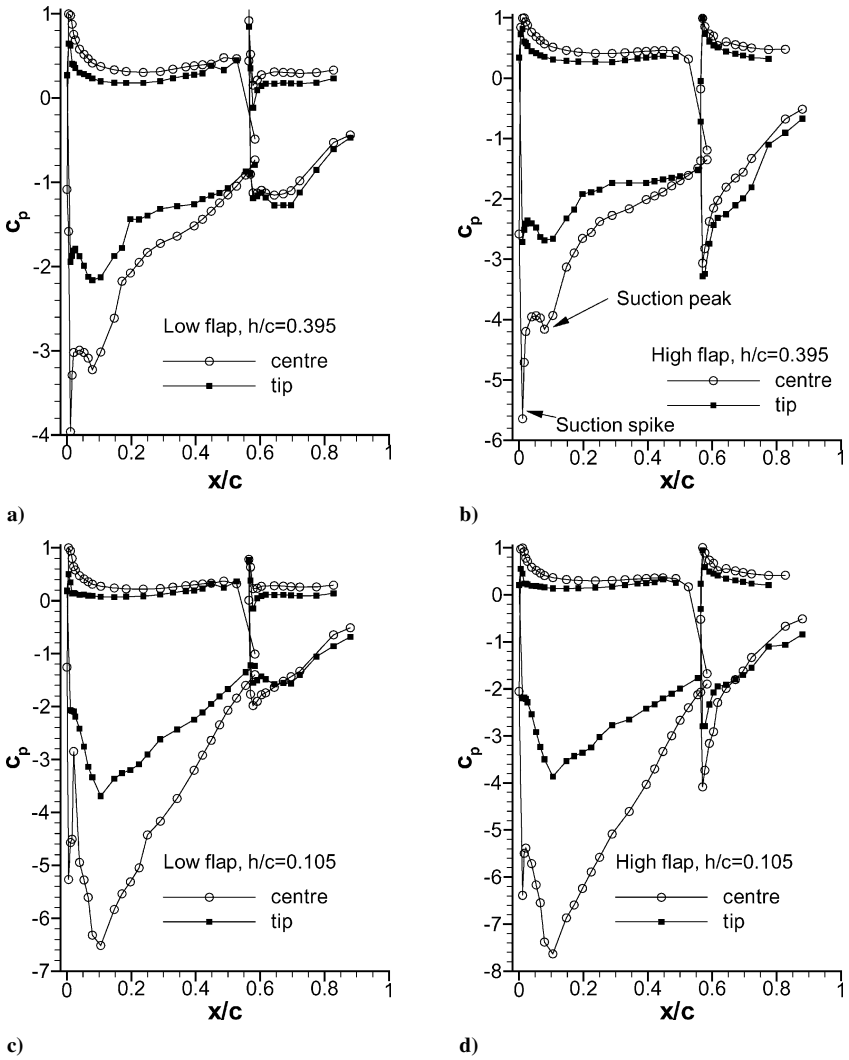

Fig. 10 Chordwise surface pressures at center and near wing tip: a) low flap angle, region A; b) high flap angle, region A; c) low flap angle, region B; and d) high flap angle, region B.

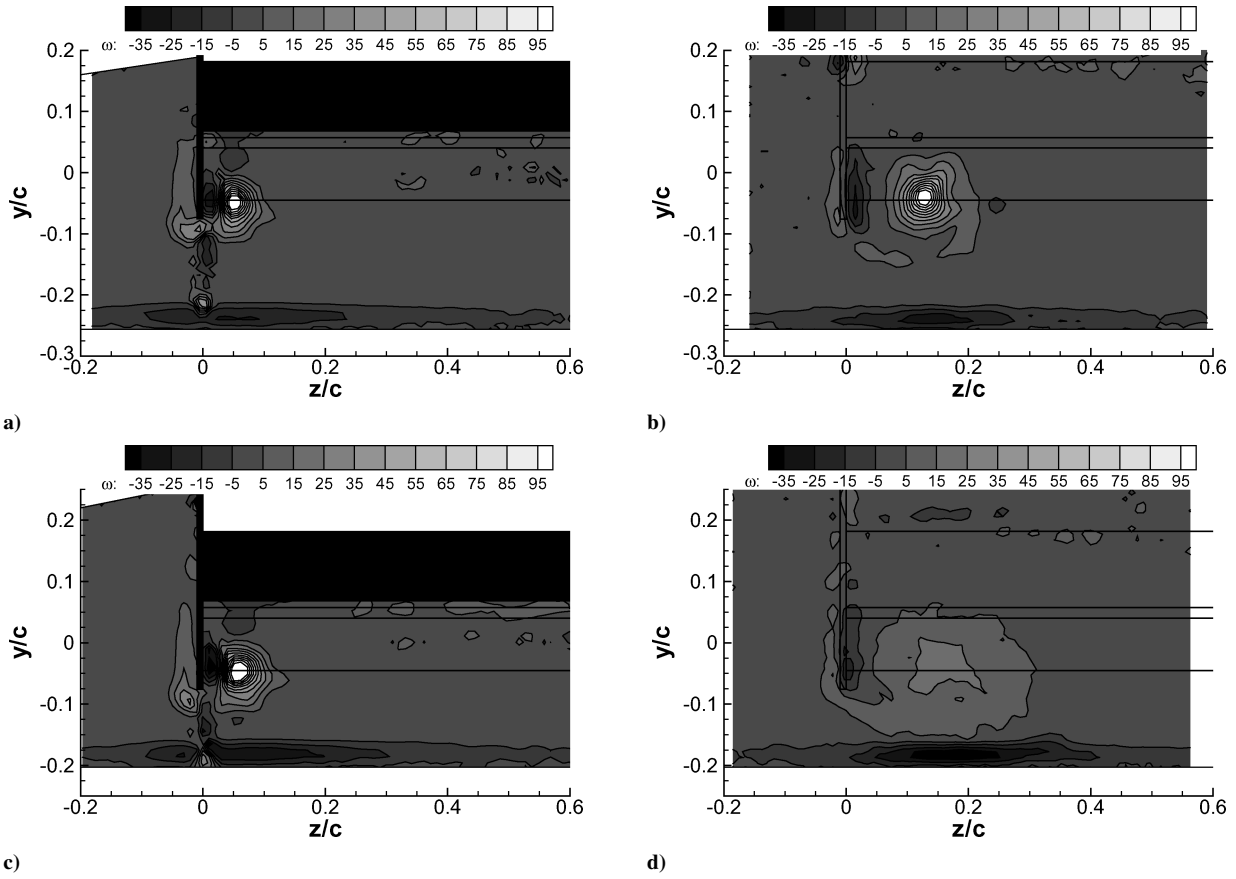

Fig. 11 Mean vorticity contours at low flap angle: a) $h/c = 0.211$, $x/c = 0.672$; b) $h/c = 0.211$, $x/c = 1.092$; c) $h/c = 0.158$, $x/c = 0.672$; and d) $h/c = 0.158$, $x/c = 1.092$.

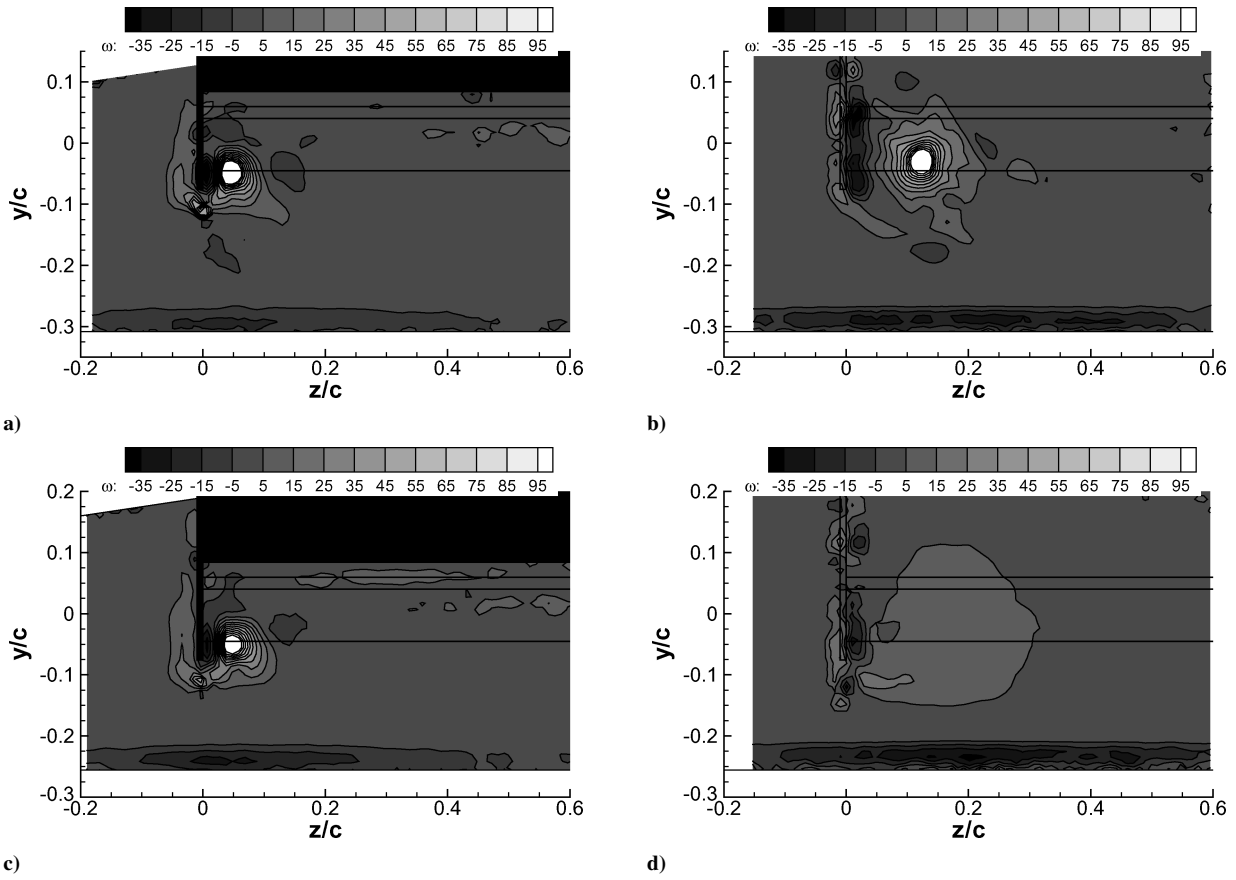

Fig. 12 Mean vorticity contours at high flap angle: a) $h/c = 0.263$, $x/c = 0.672$; b) $h/c = 0.263$, $x/c = 1.092$; c) $h/c = 0.211$, $x/c = 0.672$; and d) $h/c = 0.211$, $x/c = 1.092$.

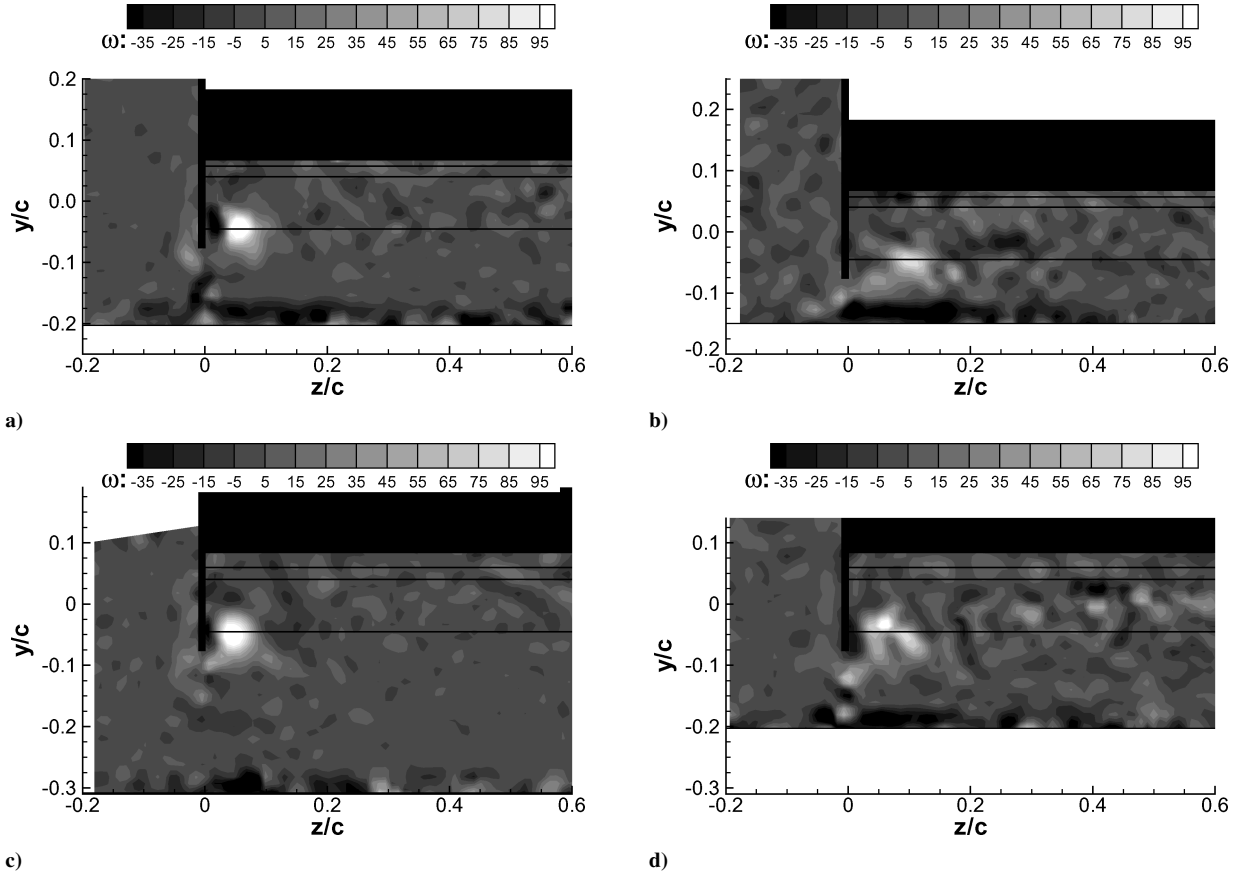

Fig. 13 Instantaneous vorticity contours: (a) low flap angle, $h/c = 0.158$, $x/c = 0.672$; (b) low flap angle, $h/c = 0.105$, $x/c = 0.672$; (c) high flap angle, $h/c = 0.263$, $x/c = 0.672$; and (d) high flap angle, $h/c = 0.158$, $x/c = 0.672$.

in the core was measured as $\omega = 153$. This is approximately 50% stronger than that for the low flap angle at this height and streamwise location. The core seems to be in a similar location compared to the low flap angle. Behind the endplate, a comparable vortex strength is again obtained at $\omega = 147$. In a manner similar to the results at the low flap angle, the rollup has been mapped quite well. The core has moved inboard and is at approximately $z/c = 0.12$, $y/c = -0.03$. Again, it is difficult to be entirely certain, but it appears that the core is a little farther inboard, and a little higher, compared to the low flap angle. The outer edge of the vortex, farthest away from the wing tip, lies farther inboard than that at the low flap angle. Also, the strength of the negative vorticity shear on the ground and that arising from the inner surface of the endplate are stronger than both that farther upstream and that at the low flap angle.

At $h/c = 0.211$ (Figs. 12c and 12d) in region B, the quarter-chord measurement indicates that a concentrated vortex exists. The maximum vorticity is measured at 126. However, behind the endplate, the strength of the vortex is reduced significantly. At a lower height of $h/c = 0.158$ (region B), the results at the quarter-chord show that the vortex has now deteriorated at this height (not included in the figure). A moderate strength of $\omega = 53$ was measured. There is, however, still a strong region of negative vorticity close to the ground, which can also be observed behind the endplate. Lower still, at $h/c = 0.105$, results similar to those for the low flap angle are again seen, with a weak area of positive vorticity for the results at the quarter-chord, which form a layer behind the endplate.

For heights near the region A/B flow boundary, the maximum vorticity found in the core has been added to Fig. 5.

2. Instantaneous Flow

For the low flap angle, at a typical height of $h/c = 0.158$ (region A), an instantaneous snapshot is given in Fig. 13a. The image features some noise. This may either be due to a real flow phenomenon, such as turbulence, or the experimental conditions, such as a lack of seeding, a reflection, or a light intensity reduction due to the microscope slide. For all snapshots taken, the vortex seems to be of the same size and location, and the strengths are also comparable. Again the results all show a concentrated vortex, which is fed by the shear layer, rolling up over the bottom edge of the endplate.

At $h/c = 0.105$ (region B), the mean flow results exhibit a sudden reduction in vortex strength (Fig. 13b), and the vortex is diffused over a large region. For the mean flow results, a maximum vorticity of $\omega = 30$ was measured at a location of $z/c = 0.08$, $y/c = -0.09$. The flow exhibited a large amount of unsteadiness with different images showing differing flows. The snapshot presented, however, is typical of the flowfield. In the bottom left of the figure, there is a region of positive vorticity that does not appear to be regular in terms of the shape and vorticity distribution. The core of the vortex is not readily apparent; however, the peak vorticity is measured as $\omega = 52$ at $z/c = 0.07$, $y/c = -0.10$. The core position experiences movement and the strength varies.

For the high flap angle (region A), the characteristics of a regular vortex with the strong core for the mean flow results are replicated in each of the instantaneous images. Two typical snapshots are given as Figs. 13c and 13d. At $h/c = 0.263$ in region A (Fig. 13c), the maximum vorticity from the mean flow results is $\omega = 153$. Of the large number of images taken, no images with a significantly reduced strength are found at $h/c = 0.263$. At a lower height of $h/c = 0.211$ in region B (not shown), the maximum vorticity from the mean flow results is $\omega = 126$, less than that at $h/c = 0.263$. Significant variations are observed among the snapshots. Typical of 90–95% of the samples taken, there exists a maximum vorticity around $\omega = 135$. For about 5–10% of all of the snapshots, there is a significant reduction in strength, to $\omega = 78$, but it is at the same location.

At a height of $h/c = 0.158$ in region B (Fig. 13d), the flow is highly unsteady and fluctuating between different states. The instantaneous results have a maximum vortex strength greater than the average due to the variation in location of the core. At $h/c = 0.105$

(not shown), mean flow results do not show the presence of a discrete core; the vortex is weak. The instantaneous images all show a highly unsteady flowfield. However, unlike the case at $h/c = 0.158$, where the vortex is unsteady but fluctuating between strong regular core, strong irregular core, and weak irregular core, all the results at $h/c = 0.105$ show an irregular edge vortex.

Behind the wing, similar connections can be found between the mean and instantaneous results.

V. Discussion

Spanwise pressures suggest that on the main element at the quarter-chord the flow increases three-dimensional for all heights as the height is reduced. On the flap, there is an increase in suction near the tip. In region A heights, the suction near the tip of the flap increases as the height is reduced. The maximum suction near the flap tip is at the lowest region A height for both flap angles. The suction near the flap tip then reduces as the ground is approached through the region B heights. This is found to be the case for the low and high deflection angles (Fig. 5).

Mean flow results on the edge vortex at the flap quarter-chord position show us that the strongest vortex here occurs at the lowest region A height for both flap angles, correlating with the surface pressures at the same location. In region B heights, the vortex strength at this location first reduces a little, then drops more significantly as the height is reduced. The results taken behind the trailing edge are a little different. The vortex strength increases as the height is reduced for the region A heights. However, there is a rapid reduction in strength for all region B heights for both the flap angles. Hence, at the largest region B height for both flap angles, the vortex at the flap quarter-chord is still relatively strong but less than its maximum, and when it has reached the measurement point behind the trailing edge, the strength is reduced significantly and a weak, diffuse vortex exists. For the remainder of region B heights, a weak vortex exists at both locations (Fig. 5).

For all region A heights, the vortex is steady, regular, and strong in all images at both locations. As the height reduces throughout region A, the strength increases such that at the smallest region A height, the vortex is stronger than at all other heights for each of the locations. At the largest region B height for the low flap angle, $h/c = 0.158$, the instantaneous images at the quarter-chord still appear to show a regular and strong vortex for all the images. For the high flap angle at the largest region B height, $h/c = 0.211$, approximately 5–10% of the images show a vortex of significantly reduced strength that has burst intermittently at the quarter-chord. For each of these heights, that is, $h/c = 0.158$ for the low flap angle and $h/c = 0.211$ for the high flap angle, the vortex bursts by the time it is at the second measurement point behind the trailing edge for all images if it has not already done so. At a lower height in region B, $h/c = 0.105$ for the low flap angle, at the quarter-chord position the instantaneous images show a weaker vortex, which is of uneven distribution and changes location according to time. The vortex has burst for all samples. For a similar region B height for the high flap angle, $h/c = 0.158$, some of the images show a strong, regular vortex, and some show a vortex that has burst (Fig. 5).

It is assumed that a strong regular vortex, as found for a region A height, will have a high-speed vortex core. This will induce greater velocities in the region near the tip of the flap. As the strength increases as the height is reduced in region A, the suction imparted near the flap tip will increase. As the vortex bursts in the region B flows, the suction near the flap tip reduces, causing the loading near the tip to reduce.

One reason for the vortex bursting may be due to the direct influence of the ground. Results show that at $h/c = 0.211$ for the high flap angle at the quarter-chord, the flow features a strong vortex, for which the vortex occasionally bursts. It can be seen that, from the mean flow results, there is a finite distance between the shear feeding the vortex rollup and the induced shear on the ground, which is of opposite direction. The reason for the vortex bursting, therefore, is not due to a merging between the main vortex and the ground (or the induced shear above the ground). For the same height, behind the trailing edge, the mean and the unsteady results again show that there is a finite distance between the (already burst) vortex and the shear above the ground. It is possible that farther downstream there may be direct interaction between the vortex and the shear above the ground, given the growth of the vortex. However, it is unlikely that this is the cause for the vortex to burst. The location at which the vortex bursts is upstream of $x/c = 1.092$ and generally downstream of $h/c = 0.672$ for the largest region B height, although the burst occasionally moves upstream of this.

Vortex breakdown has been observed in many aeronautical studies, for example for vortices over delta wings,[19] and also for rectangular wings.[19,20] The phenomenon occurs when a vortex is under an adverse pressure gradient, as would be expected for the current study. For a fixed ground height, it is clear that the adverse pressure gradient for the high flap angle would be greater than for the low flap angle. This would explain why the breakdown occurs at a greater height for the high flap angle than for the low flap angle. The location of the breakdown has been frequently observed to oscillate about position, as can be seen in the current results, where some instantaneous images show a burst vortex and some show a regular and strong vortex. When vortex breakdown occurs, this results in a rapid deceleration in the axial velocity of the vortex. Near the flap tip, for region B heights, surface pressures indicate a reduction in the suction, due to the reduction in vortex strength, and lower induced velocities.

For a strong vortex, the high axial velocity induces a large suction on the lower surface near the tip of the flap. When the vortex breakdown occurs, there is a reduction in the suction near the flap tip. Before breakdown, the vortex strength for the high flap angle is greater than that for the low flap angle. The suction that it induces is also greater for the high flap angle. When breakdown occurs, there is a reduction in local loading for the low flap angle resulting in a plateau in the downforce level. For the high flap angle there is a greater effect, and there is a sharp reduction in overall downforce for the wing.

The oil flow tests also show greater crossflows near the trailing edge of the flap in the presence of a strong edge vortex, as well as evidence of edge vortex breaking down on the surface of the wing.

The surface pressure distribution on the suction surface shows a suction peak at around $x/c = 0.08$–0.1 (Fig. 10). This is known as the suction *peak*. However, a suction *spike* near the leading edge at $x/c = 0.01$–0.02 becomes apparent when the flap is added. The spike grows for the higher flap angle. It seems that, near the tip, the suction spike is significantly reduced when compared to the center. Other researchers[27] have shown that for a two-dimensional wing with a leading-edge suction peak, the peak is virtually eliminated for a low-aspect-ratio three-dimensional case. Hence, it is likely that the reduction in the spike near the tip is directly due to the tip effects. As the height of the wing is reduced, the suction at the lowest point on the surface near the suction peak increases significantly. The suction at the spike, however, changes very little. In this manner, a large height may give the maximum suction on the main element at the center in the spike and near the tip in the peak. As the height is reduced, the suction at the peak increases, and that at the spike remains relatively constant such that, closer to the ground, the maximum suction at the center changes to the peak from the spike and that at the tip remains at the peak. Hence, the transition, occurring after the peak suction, tends to occur in the center of the wing at large heights with this region reducing as the height reduces. The larger spike with the higher flap angle promotes the leading-edge transition at the suction spike for a greater range of heights.

VI. Summary

A study was performed of three-dimensional features and edge vortices associated with a double-element wing in ground effect. The flow on the main element is highly three-dimensional near the tip. Near the tip of the wing, the contribution to the total downforce from the main element is significantly reduced compared to that at the center. The total downforce-vs-height curve is divided into three distinct regions according to ground proximity and flap settings. The three regions are characterized by 1) force enhancement and concentrated edge vortices, 2) force enhancement and vortex breakdown,

and 3) loss of downforce and separation on the wing. The gradient of the downforce-vs-height curve shows a sudden change between regions A and B. The edge vortex from the main element induces a region of high suction near the tip of the flap. When the vortex is strong (region A), the flap produces more downforce at the tip than at the center. In region B flows, the edge vortex breaks down, resulting in a loss of downforce near the tip of the flap and, hence, changing the curve of the downforce. The study establishes a link between the formation/behavior of the edge vortex and the force/pressure behaviors.

References

[1]Zhang, X., and Zerihan, J., "Aerdynamics of a Double Element Wing in Ground Effect," *AIAA Journal*, Vol. 41, No. 6, 2003, pp. 1007–1016.

[2]Knowles, K., Donahue, D., and Finnis, M., "A Study of Wings in Ground Effect," *Loughborough University Conference on Vehicle Aerodynamics*, The Royal Aeronautical Society, London, UK, July 1994, pp. 22.1–22.13.

[3]Ranzenbach, R., Barlow, J., and Diaz, R., "Multi-Element Airfoil in Ground Effect—An Experimental and Computational Study," AIAA Paper 97-2238, June 1997.

[4]Jasinski, W., and Selig, M., "Experimental Study of Open-Wheel Race-Car Front Wings," Society of Automotive Engineers, Publ. 983042, Nov. 1998.

[5]Zerihan, J., and Zhang, X., "Aerodynamics of a Single-Element Wing-in-Ground Effect," *Journal of Aircraft*, Vol. 37, No. 6, 2000, pp. 1058–1064.

[6]Zerihan, J., and Zhang, X., "Unsteady Turbulent Wake Behind a Single-Element Wing in Ground Effect," *10th International Symposium on Applications of Laser Techniques to Fluid Mechanics*, Lisbon, July 2000, p. 8-1.

[7]Olson, L., and Orloff, K., "On the Structure of Turbulent Wakes and Merging Shear Layers of Multi-Element Airfoils," AIAA Paper 81-1238, June 1998.

[8]Adair, D., and Clifton, H., "Turbulent Separated Flow in the Vicinity of a Single-Slotted Airfoil Flap," AIAA Paper 88-0613, Jan. 1988.

[9]Nakayama, A., Kreplin, H.-P., and Morgan, H., "Experimental Investigation of Flowfield About a Multielement Airfoil," *AIAA Journal*, Vol. 28, No. 1, 1990, pp. 14–21.

[10]Biber, K., and Zumwalt, G., "Flowfield Measurements of a Two-Element Airfoil with Large Separation," *AIAA Journal*, Vol. 31, No. 3, 1993, pp. 459–464.

[11]Smith, A., "High-Lift Aerodynamics," *Journal of Aircraft*, Vol. 12, No. 6, 1975, pp. 501–530.

[12]Baker, G., Barker, S., Bofha, K., and Saffman, P., "Laser Anemometer Measurements of Trailing Vortices in Water," *Journal of Fluid Mechanics*, Vol. 65, 1974, pp. 325–336.

[13]Green, S., and Acosta, A., "Unsteady Flow in Trailing Vortices," *Journal of Fluid Mechanics*, Vol. 227, 1991, pp. 107–134.

[14]Ramaprian, B., and Zhang, Y., "Measurements in Rollup Region of the Tip Vortex from a Rectangular Wing," *AIAA Journal*, Vol. 35, No. 12, 1997, pp. 1837–1843.

[15]Khorrami, M. R., Singer, B., and Radeztsky, R. J., "Reynolds-Averaged Navier–Stokes Computations of a Flap-Side-Edge Flowfield," *AIAA Journal*, Vol. 37, No. 1, 1999, pp. 14–22.

[16]Snyder, D., and Spall, R., "Numerical Investigation into Multiple Vortex Structures Formed over Flat End-Cap Wings," *AIAA Journal*, Vol. 38, No. 8, 2000, pp. 1486–1489.

[17]Polhamus, E., "Predictions of Vortex-Lift Characteristics by a Leading-Edge Suction Analogy," *Journal of Aircraft*, Vol. 8, No. 4, 1971, pp. 193–199.

[18]Wentz, W., Jr., and Kohlman, D., "Vortex Breakdown on Slender Sharp-Edged Wings," *Journal of Aircraft*, Vol. 8, No. 3, 1971, pp. 156–161.

[19]Payne, F., Ng, T., Nelson, R., and Schiff, L., "Visualisation and Wake Surveys of Vortical Flow Over a Delta Wing," *AIAA Journal*, Vol. 26, No. 2, 1988, pp. 137–143.

[20]Delery, J., "Aspects of Vortex Breakdown," *Progress in Aerospace Sciences*, Vol. 30, 1994, pp. 1–59.

[21]Gursul, I., and Xie, W., "Origin of Vortex Wandering over Delta Wings," *Journal of Aircraft*, Vol. 37, No. 2, 2000, pp. 348–350.

[22]Harvey, J., and Perry, F., "Flowfield Produced by Trailing Vortices in the Vicinity of the Ground," *AIAA Journal*, Vol. 9, No. 8, 1971, pp. 1659, 1660.

[23]Storms, B., Takahashi, T., and Ross, J., "Aerodynamic Influence of a Finite-Span Flap on a Simple Wing," Society of Automotive Engineers, Publ. 951977, Sept. 1995.

[24]Radeztsky, R., Jr., Singer, B., and Khorrami, M., "Detailed Measurements of a Flap Side-Edge Flow Field," AIAA Paper 98-0700, Jan. 1998.

[25]Takallu, M., and Laflin, K., "Reynolds-Averaged Navier–Stokes of Two Partial-Span Flap Wing Experiments," AIAA Paper 98-0701, 1998.

[26]Mathias, D., Roth, K., Ross, J., Rogers, S., and Cummings, R., "Navier–Stokes Analysis of the Flow about a Flap Edge," *Journal of Aircraft*, Vol. 35, No. 6, 1998, pp. 833–838.

[27]Katz, J., "Aerodynamics of High-Lift Low Aspesct-Ratio Unswept Wings," *AIAA Journal*, Vol. 27, No. 8, 1989, pp. 1123, 1124.